# Multiferroic materials based on transition-metal dichalcogenides: Potential platform for reversible control of Dzyaloshinskii-Moriya interaction and skyrmion via electric field

Ziji Shao,[1,2] Jinghua Liang,[1] Qirui Cui,[1] Mairbek Chshiev,[3,4] Albert Fert,[5] Tiejun Zhou,[2,*] and Hongxin Yang[1,†]

[1]*Ningbo Institute of Materials Technology and Engineering, Chinese Academy of Sciences, Ningbo 315201, China and Center of Materials Science and Optoelectronics Engineering, University of Chinese Academy of Sciences, Beijing 100049, China*

[2]*College of Electronics and Information, Hangzhou Dianzi University, Hangzhou 310018, China*

[3]*Univ. Grenoble Alpes, CEA, CNRS, Spintec, 38000 Grenoble, France*

[4]*Institut Universitaire de France, 75231 Paris, France*

[5]*Université Paris-Saclay, Unité Mixte de Physique CNRS-Thales, Palaiseau 91767, France*

(Received 1 June 2021; revised 23 March 2022; accepted 19 April 2022; published 9 May 2022)

Exploring novel two-dimensional multiferroic materials that can realize electric-field control of two-dimensional magnetism has become an emerging topic in spintronics. Using first-principles calculations, we demonstrate that nonmetallic bilayer transition-metal dichalcogenides can be an ideal platform for building multiferroics by intercalated magnetic atoms. Moreover, we unveil that with Co intercalated bilayer $MoS_2$, $Co(MoS_2)_2$, two energetically degenerate states with opposite chirality of Dzyaloshinskii-Moriya interaction are the ground states, indicating electric-field control of the chirality of topological magnetic objects such as skyrmions can be realized in this type of materials by reversing the electric polarization. These findings pave the way for electric-field control of topological magnetism in two-dimensional multiferroics with intrinsic magnetoelectric coupling.

DOI: 10.1103/PhysRevB.105.174404

## I. INTRODUCTION

The manipulation of spin is the base of spintronic devices with new capabilities and potentially superior performance [1]. Electric control of magnetism is considered to be an efficient approach for applications with low energy consumption and high-speed magnetic switching. Chiral magnetic structures such as chiral domain walls [2,3], helical structures [4,5], and magnetic skyrmions [6–8] which generally originate from Dzyaloshinskii-Moriya interactions (DMIs) are highly promising for next generation spintronic devices and are required to be electrically controllable for integration into modern electronic technology [9–11]. It has been reported that electric control of skyrmions can been realized by spin-polarized current based on spin-transfer torque or spin-orbit torque effects [12–16]. However, for industrial applications, ultralow electric current threshold to move domain walls and skyrmions is demanded to reduce energy consumption [17]. It was suggested that the coupling between magnetism and electric polarization (ME) allows the manipulation of magnetization through an electric field with low power consumption [18–23]. Two-dimensional (2D) ferromagnetic materials with broken inversion symmetry may provide a promising opportunity to control their DMI [24–27]. Due to ME coupling, the DMI and topological magnetic structure switching mediated by an electric field is found in multiferroic $VOI_2$ monolayer [28] and $Ca_3FeOsO_7$ bilayer [29], but no skyrmions are obtained in these systems. Recently, the transformation between four states of skyrmions controlled by an out-of-plane electric field was demonstrated in CrN monolayer theoretically [24], guiding towards realization of the electric-field manipulation of the topological chirality and promoting further explorations of novel multiferroic materials allowing electric control of skyrmions [30].

A class of covalently bonded self-intercalated bilayer transition-metal dichalcogenides (TMDs) are successfully synthesized recently using both molecular beam epitaxy (MBE) and chemical vapor deposition methods [31]. The term ic-2D crystals has been coined for structures such as $TaS_2$-Ta-$TaS_2$ grown by MBE [31]. By varying the coverage of the intercalated metal from low concentration to complete intercalation with the intercalated atoms occupying the octahedral vacancies between the two S layers, the magnetic properties can be tuned. In addition, experimental results have shown that $CoMoS_2$ presents ferromagnetic properties with out-of-plane magnetization and Curie temperature $T_c$ around 100 K [32].

Herein, we propose that the bilayer TMDs can serve as an efficient platform for forming 2D multiferroic systems with intrinsic ME coupling, such as Co intercalated bilayer $MoS_2$. The intercalated Co atoms not only introduce the magnetism but also induce ferroelectricity via the formation of polar structure. Therefore, an external electric field can alter the magnetic properties when reversing the electric polarization. The first-principles calculations suggest two equivalent multiferroic phases of $Co(MoS_2)_2$ (denoted as FE1 and FE2) with opposite chirality of DMI. Moreover, the chirality of skyrmions can be controlled by a vertically applied electric field in $Co(MoS_2)_2$.

*tjzhou@hdu.edu.cn
†hongxin.yang@nimte.ac.cn

 

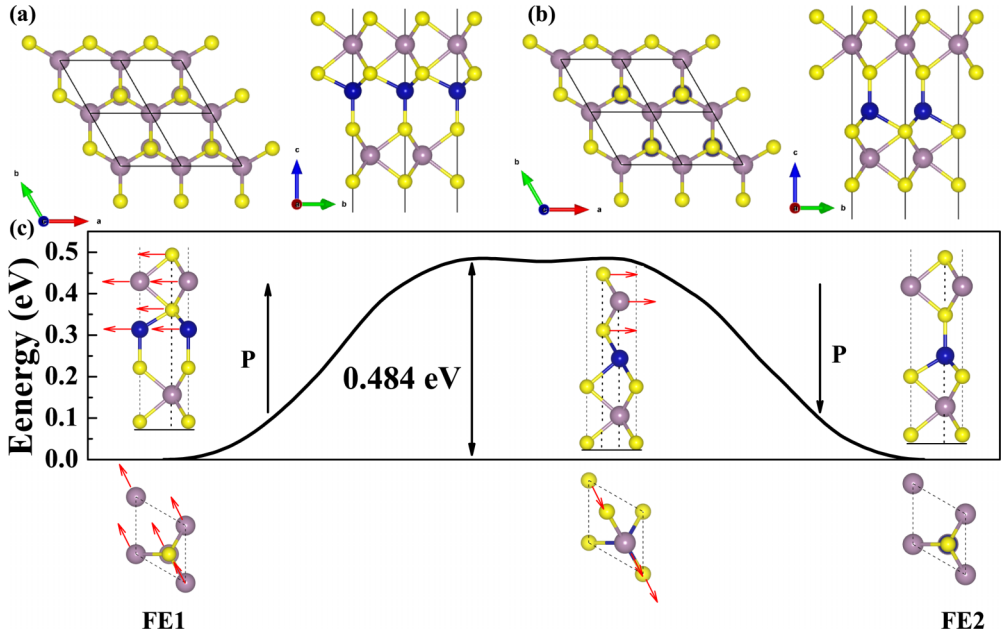


FIG. 1. The top (left) and side (right) views of the (a) FE1 and (b) FE2 phases of $Co(MoS_2)_2$ monolayer. Blue, pink, and yellow balls represent Co, Mo, and S atoms, respectively. (c) The ferroelectric switching pathway of $Co(MoS_2)_2$ by the NEB method with the top and side views of the transition structure during the ferroelectric switching. The red arrows depicted the orientation of atomic movement.

## II. COMPUTATIONAL METHODS

The first-principles calculations are performed in the framework of density-functional theory (DFT) [33] as implemented in the Vienna *ab initio* Simulation Package (VASP) [34]. The electron-ion interaction is described through the projected augmented wave method [35–37], and the electronic exchange-correlation functional is treated by the generalized gradient approximation (GGA) parametrized by Perdew, Burke, and Ernzerhof (PBE) [38]. In order to well describe the $3d$ electrons, we employ the GGA+$U$ method [39] with an effective $U_{\text{eff}} = 3$ eV for $3d$ orbitals of Co atoms [40,41]. The plane-wave cutoff energy is set to 500 eV. The first Brillouin zone is sampled by a Γ-centered $25 \times 25 \times 1$ $k$-point mesh. Structural relaxations are performed until the forces become smaller than 0.001 eV/Å per atom. The phonon dispersion is calculated using density-functional perturbation theory [42], as implemented in the PHONOPY code [43,44]. The magnetic anisotropy energy $K$ can be obtained by calculating the energy difference between in-plane [100] and out-of-plane [001] magnetization orientations taking into account spin-orbit interaction. Heisenberg exchange coupling $J$ is calculated by comparing the energies between ferromagnetic and antiferromagnetic states [25]. We employ the chirality-dependent total energy difference approach to calculate the DMI constant $d$. This method has been successfully applied on Co/Pt film [45,46], Co/MgO [46,47], Co/graphene [48], and 2D magnetic materials such as Mn$XY$, Cr$XY$ with XY representing chalchogen atoms, as well as CrN [24–26]. The details are shown in the Supplemental Material [49]. A Γ-centered $6 \times 6 \times 1$ $k$-point mesh is adopted in the calculations of DMI. A positive $d$ indicates the anticlockwise (ACW) spin configurations while a negative $d$ is a clockwise (CW) one.

## III. RESULTS AND DISCUSSION

We first systematically investigate all the possible atomic configurations [Fig. S1(a) of the Supplemental Material [49]] of $Co(MoS_2)_2$ using DFT calculations. The geometry of $Co(MoS_2)_2$ structures can be seen as two $MoS_2$ layers intercalated by one layer of Co atoms. From the calculated total energy dependence as a function of lattice constant for each structure [Fig. S1(b) of the Supplemental Material [49]], we find that the energetically degenerate ferroelectric phases FE1 and FE2 are the ground states. The dynamical stability is confirmed through phonon calculation and *ab initio* molecular dynamic simulation [Fig. S2 of the Supplemental Material [49]]. The structures of the FE1 and FE2 phases are depicted in Figs. 1(a) and 1(b) with optimized lattice constant 3.224 Å. Each Co atom is tetra-coordinate and occupies the trigonal-pyramidal vacancies between two stacking $MoS_2$ layers. The electron localization functions (ELFs) (Fig. S3 of the Supplemental Material [49]) indicate the mixture of covalent and ionic interactions between Co and the adjacent S. This tetra-coordinate environment causes different vertical distances between Co atoms and two adjacent $MoS_2$ monolayers, which induces the electric polarization. The electric dipoles of the stable ferroelectric states FE1 and FE2 are calculated to be $0.029e$ Å/f.u. and $-0.029e$ Å/f.u., respectively. The reversion of the electric polarization can be realized via the displacement of the Co atom [54]. The ferroelectric switching pathways are investigated by using the nudged elastic band (NEB) method [55]. Here, we adopt a two-step switching path with a metastable phase being the transition state. In many theoretical studies, this kind of multistep switching path can efficiently reduce the energy of barriers [56]. As shown in Fig. 1(c), the FE1 phase first converts into the transition phase via shifting the top four atomic layers along a diagonal as

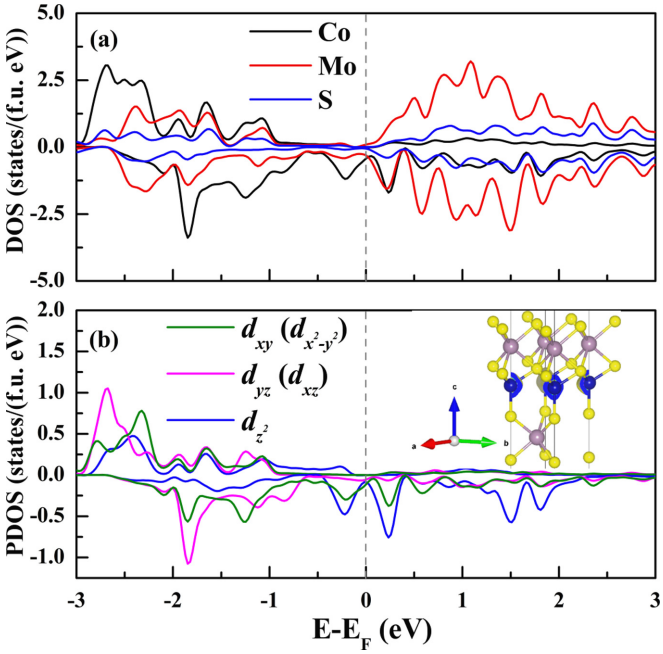


FIG. 2. (a) The atom-projected partial PBE for $Co(MoS_2)_2$ monolayer. (b) The atomic orbital-projected DOS for each $d$ orbital of the Co atom in $Co(MoS_2)_2$ monolayer. The spin density of $Co(MoS_2)_2$ monolayer is shown in the inset; the blue, pink, and yellow balls represent the Co, Mo, and S atoms, respectively.

illustrated by the red arrows. Then the top $MoS_2$ monolayer of the transition phase moves back to the original position to realize the transformation from the transition phase to the FE2 phase. The overall switching barrier is calculated to be 0.484 eV/f.u. [Fig. 1(c)].

The partial electronic density of states (PDOS in Fig. 2) provides two important pieces of information of $Co(MoS_2)_2$ monolayer. First, the existence of electronic density at the Fermi level indicates a metallic characteristic for ferroelectric $Co(MoS_2)_2$. Therefore, the electrons are confined within the slab and only vertical polarization exists [57]. Second, $Co(MoS_2)_2$ is ferromagnetic, which is mainly induced by intercalated Co atoms. The magnetic moment is calculated to be about $1.28\mu_B$ per Co atom. The atomic-projected electronic density of states [Fig. 2(b)] and spin density [inset in Fig. 2(b)] show that the magnetism is mainly caused by the partial occupation of the $dz^2$, $d_{xy}$, and $dx^2 - y^2$ states of Co atoms. Since the spin polarization is mainly provided by Co atoms, the following Hamiltonian model is employed in systems considered here for further investigating the magnetic properties:

$$H = -J\sum_{i,j} \boldsymbol{S}_j \cdot \boldsymbol{S}_j - K\sum_i \left(S_i^z\right)^2 + \sum_{i,j} \boldsymbol{D}_{i,j} \cdot (\boldsymbol{S}_i \times \boldsymbol{S}_j) - \mu_{Co} B \sum_i S_i^z, \quad (1)$$

where $\boldsymbol{S}_i$ indicates the spin unit vector of the $i$th Co atom. Here, we only take the magnetic coupling between the

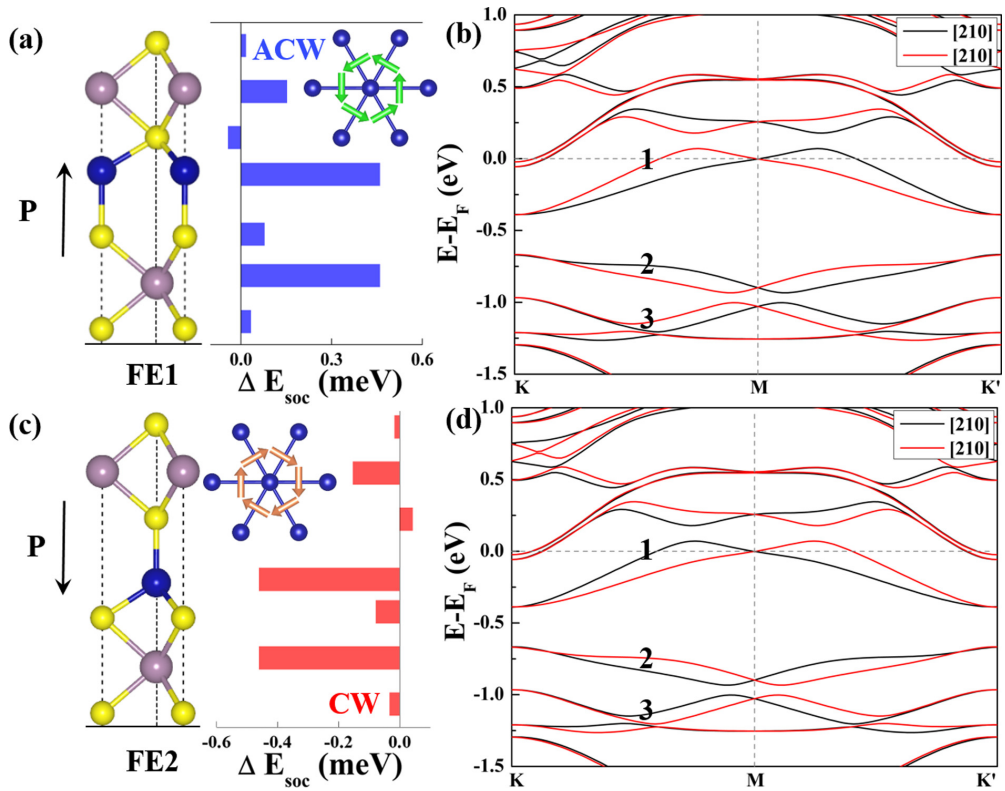


FIG. 3. Atom-resolved localization of the DMI associated SOC energy $\Delta E_{SOC}$ in $Co(MoS_2)_2$ monolayer with (a) up and (c) down electric polarization. Band structures of (b) up and (d) down polarized $Co(MoS_2)_2$ monolayer with the magnetization direction along [210] (black lines) and $[\bar{2}\bar{1}0]$ (red lines). Three bands under the Fermi level (bands 1, 2, and 3) are chosen to estimate the $D_R$ value.

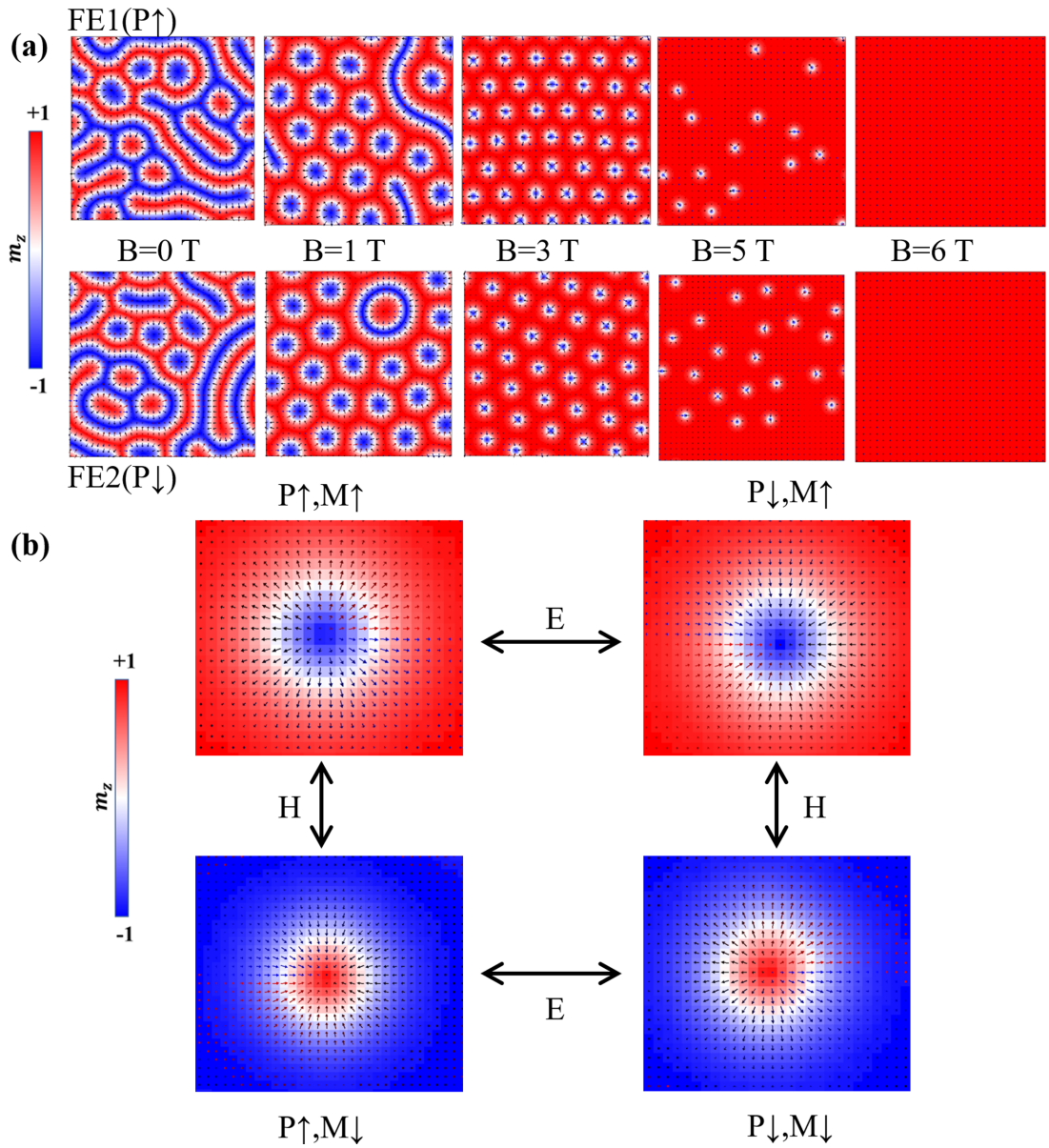


FIG. 4. (a) Spin textures for $Co(MoS_2)_2$ in real space under 0, 1, 3, 5, and 6 T in the FE1 and FE2 phases. The color map indicates the out-of-plane spin component of Co atoms. Panel (b) illustrates the realization of the switching of four types of skyrmions ($P\uparrow$, $M\uparrow$), ($P\uparrow$, $M\downarrow$), ($P\downarrow$, $M\uparrow$), and ($P\downarrow$, $M\downarrow$) with different chirality and polarity via an external field, similar to that in CrN [24]. $M$ and $P$ represent the magnetization and electric polarization, respectively. ACW and CW are anticlockwise and clockwise.

nearest Co atoms into consideration; therefore $i$, $j$ represent the nearest neighbor Co atom pairs. The first three terms correspond to DMI, Heisenberg exchange coupling, and single-ion anisotropy, characterized by $\boldsymbol{D}_{i,j}$, $J$, and $K$, respectively. The specific calculation method is given in the Supplemental Material [49]. The last term represents the Zeeman interaction with $\mu_{Co}$ and $B$ being magnetic moment of the Co atoms and the external magnetic field, respectively. The magnetic ground states of ferroelectric $Co(MoS_2)_2$ are calculated to be ferromagnetic out of plane with the nearest neighbor magnetic interaction parameter $J$ about 5.65 meV and the perpendicular magnetic anisotropy (PMA) about 0.09 meV, respectively. The broken inversion symmetry induced by tetra-coordinate Co atoms provides an opportunity for the appearance of a chiral domain wall or skyrmions in the case of significant spin-orbit coupling (SOC) energy sources present [58,59]. Therefore, we investigated the DMI and the associated SOC energy difference $\Delta E_{SOC}$ of these two equivalent ferroelectric phases. The DMI strengths for the FE1 and FE2 phases with up and down electric polarization are the same with values of 1.34 meV. However, their chirality is opposite, being ACW for FE1 and CW for FE2, respectively. As shown in Figs. 3(a) and 3(c), the largest associated $\Delta E_{SOC}$ originates from the Co layer and is located away from the Mo layer with both contributing equally. These results indicate that both Fert-Levy [45,60] and Rashba [48] physical mechanisms governing the DMI coexist in the Co intercalated multiferroic phase proposed here. In order to explore the

influence of Rashba SOC on the DMI [61–64], the electronic band structures with magnetization pointing along the [210] and $[\bar{2}\bar{1}0]$ directions are calculated with the SOC switched on. As shown in Figs. 3(b) and 3(d), the significant Rashba-type **k**-dependent splitting indicates large Rashba effect in this system. To quantitatively estimate its contribution to the total DMI, the Rashba-type DMI parameter $D_R$ is estimated with $D_R = (\frac{4m^*A}{\hbar^2})\alpha_R$ [61], where $m^*$ indicates the effective mass of electron, $\alpha_R$ is the Rashba coefficient which can be extracted from equation $\alpha_R = 2\Delta E/\Delta k$, and $A$ represents the exchange stiffness estimated to be 2.45 meV Å$^2$/f.u. in $Co(MoS_2)_2$ [65]. Here we mainly focus on three bands [1, 2, and 3 shown in Figs. 3(b) and 3(d)] around the $M$ point along the $K$-$M$-$K'$ path under the Fermi level. In terms of the oblivious band shifts, the Rashba coefficient $\alpha_R$ is estimated to be 0.779, 1.048, and 0.908 eV Å for bands 1, 2, and 3 with effective masses $m^*$ equal to 5.07, −8.27, and 5.65 in units of the rest mass of electron $m_e$, respectively. The corresponding magnitudes of $D_R$ evaluated from these parameters are 5.17, −11.35, and 6.74 meV Å/f.u. This allows estimating the total $D_R$ resulting from these three bands being about 0.56 meV Å/f.u. The calculated Rashba-type $D_R$ is comparable to the half of the value obtained from DFT calculations, allowing one to conclude that the Rashba SOC has a comparable contribution to the DMI with the Fert-Levy SOC. The existence of the sizable Rashba-type DMI in the ferroelectric $Co(MoS_2)_2$ phase indicates the possibility to realize electric-field control of the chirality of topological spin structures. As shown in Fig. 3, the transition from the FE1 to the FE2 phase accompanied with the inversion of electric polarization induces the inversion of the chirality of DMI from ACW to CW due to the inversion of $\Delta E_{SOC}$ and the Rashba splitting. The results show that the electric control on the chirality of chiral magnetic structures can be realized in our multiferroic $Co(MoS_2)_2$ materials. Using all magnetic parameters estimated from the first-principles calculations listed in Table SI of the Supplemental Material [49], we performed micromagnetic simulations with 100 nm × 100 nm scale using the MUMAX3 package [66] for two ferroelectric phases FE1 and FE2 with ACW and CW DMI under different external magnetic fields, respectively. Ferromagnetic states with wormlike domains are found under 0 T magnetic field. When the magnetic field is applied, the skyrmions are induced in the range of 1–5 T, and then disappear under 6 T [Fig. 4(a)]. Furthermore, the chirality of wormlike domains and skyrmions can be switched between CW and ACW configurations through the application of an external electric field since the reversing of electric polarization allows controlling the DMI chirality (Fig. S5 of the Supplemental Material [49]). With the polarity of skyrmions **M** defined as magnetization directions in skyrmion core, we thus obtain four topological configurations interchangeable and controlled through the application of external electric and magnetic fields in $Co(MoS_2)_2$ [Fig. 4(b)].

In addition to $Co(MoS_2)_2$, we also investigated other potential candidates for the proposed ME coupling including $Co(MoSe_2)_2$, $Co(MoTe_2)_2$, and $Co(WS_2)_2$ as summarized in Table SII of the Supplemental Material [49]. All of them are ferroelectric with electronic polarizations about 0.012, 0.012, and 0.023$e$ Å/f.u., respectively. Both $Co(MoTe_2)_2$ and $Co(WS_2)_2$ have considerable DMI amplitudes of about 1.044 and 2.632 meV. These values are comparable to representative erromagnetic-metal/heavy-metal (FM/HM) heterostructures, such as Fe/Ir (111) (∼1.7 meV) [67] and Co/Pt (∼3.0 meV) [45] thin films, and the 2D magnetoelectric multiferroics CrN (∼3.74 meV) [26] in which the DMI is mainly generated either by the Fert-Levy or Rashba effect mechanism, respectively. Skyrmion states are found to exist in these systems. Even for the $Co(MoSe_2)_2$ with the weakest DMI interaction (∼0.440 meV), the value is comparable to the Rashba-type DMI in the graphene/Co system (∼0.16 meV) [48] with chiral domain walls. Therefore, Co intercalated TMD systems studied here are expected to be potential multiferroic materials with realizable chirality switching via electric field.

## IV. CONCLUSION

In conclusion, we proposed bilayer TMDs as a platform towards the realization of a novel class of 2D multiferroic materials via intercalating magnetic atoms. Intrinsic multiferroicity with ME coupling can be obtained with intercalated magnetic atoms located at the positions with different interlayer spacing between two TMD layers. Using first-principles calculations, the Co intercalated bilayer $MoS_2$, $Co(MoS_2)_2$, is found to be multiferroic with degenerate DMI for two ferroelectric states. As a result, the chirality of skyrmions can be reversed via electric field thanks to the ME coupling. We have also shown that these properties can be realized in other multiferroic TMDs with Co intercalated within bilayer $MoTe_2$ and $WS_2$ systems, i.e., $Co(MoTe_2)_2$ and $Co(WS_2)_2$. In addition, different combinations of the TMD layers can further enrich the varieties of this kind of multiferroic materials [26] like $Co(Mo_2SSe)$. Considering experimentally successful synthesis of the self-intercalated TMDs with well-developed intercalation techniques [31] and the as-exfoliated nanosheets $AgCrS_2$ with a general redox-controlled strategy [68] proposed recently, the multiferroic $Co(MoS)_2$ provides a new route towards novel two-dimensional multiferroic materials that can realize the electric control of topological magnetism in 2D spintronics.

## ACKNOWLEDGMENTS

This work was supported by Pioneer and Leading Goose R&D Program of Zhejiang Province (Grant No. 2022C01053), National Natural Science Foundation of China (Grants No. 11874059 and No. 12174405), Ningbo Key Scientific and Technological Project (Grant No. 2021000215), Zhejiang Provincial Natural Science Foundation (Grant No. LR19A040002), Beijing National Laboratory for Condensed Matter Physics (Grant No. 2021000123), and European Union's Horizon 2020 Research and Innovation Program under Grant Agreement No. 881603 (Graphene Flagship).

[1] S. S. P. Parkin, M. Hayashi, and L. Thomas, Magnetic domain-wall racetrack memory, Science **320**, 190 (2008).

[2] A. Thiaville, S. Rohart, É. Jué, V. Cros, and A. Fert, Dynamics of Dzyaloshinskii domain walls in ultrathin magnetic films, Europhys. Lett. **100**, 57002 (2012).

[3] K.-S. Ryu, L. Thomas, S.-H. Yang, and S. Parkin, Chiral spin torque at magnetic domain walls, Nat. Nanotechnol. **8**, 527 (2013).

[4] M. Bode, M. Heide, K. von Bergmann, P. Ferriani, S. Heinze, G. Bihlmayer, A. Kubetzka, O. Pietzsch, S. Blügel, and R. Wiesendanger, Chiral magnetic order at surfaces driven by inversion asymmetry, Nature (London) **447**, 190 (2007).

[5] C. S. Spencer, J. Gayles, N. A. Porter, S. Sugimoto, Z. Aslam, C. J. Kinane, T. R. Charlton, F. Freimuth, S. Chadov, S. Langridge, J. Sinova, C. Felser, S. Blügel, Y. Mokrousov, and C. H. Marrows, Helical magnetic structure and the anomalous and topological Hall effects in epitaxial B20 $Fe_{1-y}Co_yGe$ films, Phys. Rev. B **97**, 214406 (2018).

[6] A. N. Bogdanov and D. A. Yablonskiui, Thermodynamically stable "vortices" in magnetically ordered crystals. The mixed state of magnets, Zh. Eksp. Teor. Fiz. **95**, 178 (1989) [Sov. Phys. JETP **68**, 101 (1989)].

[7] S. Mühlbauer, B. Binz, F. Jonietz, C. Pfleiderer, A. Rosch, A. Neubauer, R. Georgii, and P. Böni, Skyrmion lattice in a chiral magnet, Science **323**, 915 (2009).

[8] X. Z. Yu, N. Kanazawa, Y. Onose, K. Kimoto, W. Z. Zhang, S. Ishiwata, Y. Matsui, and Y. Tokura, Near room-temperature formation of a skyrmion crystal in thin-films of the helimagnet FeGe, Nat. Mater. **10**, 106 (2011).

[9] A. Fert, N. Reyren, and V. Cros, Magnetic skyrmions: Advances in physics and potential applications, Nat. Rev. Mater. **2**, 17031 (2017).

[10] F. Matsukura, Y. Tokura, and H. Ohno, Control of magnetism by electric fields, Nat. Nanotechnol. **10**, 209 (2015).

[11] A. C. Garcia-Castro, W. Ibarra-Hernandez, E. Bousquet, and A. H. Romero, Direct Magnetization-Polarization Coupling in $BaCuF_4$, Phys. Rev. Lett. **121**, 117601 (2018).

[12] A. Fert, V. Cros, and J. Sampaio, Skyrmions on the track, Nat. Nanotechnol. **8**, 152 (2013).

[13] A. Rosch, Moving with the current, Nat. Nanotechnol. **8**, 160 (2013).

[14] Y. Zhou, Magnetic skyrmions: Intriguing physics and new spintronic device concepts, Nat. Sci. Rev. **6**, 210 (2018).

[15] W. Jiang, P. Upadhyaya, W. Zhang, G. Yu, M. B. Jungfleisch, F. Y. Fradin, J. E. Pearson, Y. Tserkovnyak, K. L. Wang, O. Heinonen, S. G. E. te Velthuis, and A. Hoffmann, Blowing magnetic skyrmion bubbles, Science **349**, 283 (2015).

[16] S. Woo, K. Litzius, B. Krüger, M.-Y. Im, L. Caretta, K. Richter, M. Mann, A. Krone, R. M. Reeve, M. Weigand, P. Agrawal, I. Lemesh, M.-A. Mawass, P. Fischer, M. Kläui, and G. S. D. Beach, Observation of room-temperature magnetic skyrmions and their current-driven dynamics in ultrathin metallic ferromagnets, Nat. Mater. **15**, 501 (2016).

[17] F. Jonietz, S. Mühlbauer, C. Pfleiderer, A. Neubauer, W. Münzer, A. Bauer, T. Adams, R. Georgii, P. Böni, R. A. Duine, K. Everschor, M. Garst, and A. Rosch, Spin transfer torques in MnSi at ultralow current densities, Science **330**, 1648 (2010).

[18] P. Huang, M. Cantoni, A. Kruchkov, J. Rajeswari, A. Magrez, F. Carbone, and H. M. Rønnow, In situ electric field skyrmion creation in magnetoelectric $Cu_2OSeO_3$, Nano Lett. **18**, 5167 (2018).

[19] C. Ma, X. Zhang, J. Xia, M. Ezawa, W. Jiang, T. Ono, S. N. Piramanayagam, A. Morisako, Y. Zhou, and X. Liu, Electric field-induced creation and directional motion of domain walls and skyrmion bubbles, Nano Lett. **19**, 353 (2019).

[20] J. S. White, K. Prša, P. Huang, A. A. Omrani, I. Živković, M. Bartkowiak, H. Berger, A. Magrez, J. L. Gavilano, G. Nagy, J. Zang, and H. M. Rønnow, Electric-Field-Induced Skyrmion Distortion and Giant Lattice Rotation in the Magnetoelectric Insulator $Cu_2OSeO_3$, Phys. Rev. Lett. **113**, 107203 (2014).

[21] P.-J. Hsu, A. Kubetzka, A. Finco, N. Romming, K. von Bergmann, and R. Wiesendanger, Electric-field-driven switching of individual magnetic skyrmions, Nat. Nanotechnol. **12**, 123 (2017).

[22] T. Srivastava, M. Schott, R. Juge, V. Křižáková, M. Belmeguenai, Y. Roussigné, A. Bernand-Mantel, L. Ranno, S. Pizzini, S.-M. Chérif, A. Stashkevich, S. Auffret, O. Boulle, G. Gaudin, M. Chshiev, C. Baraduc, and H. Béa, Large-voltage tuning of Dzyaloshinskii–Moriya interactions: A route toward dynamic control of skyrmion chirality, Nano Lett. **18**, 4871 (2018).

[23] Y. Wang, L. Wang, J. Xia, Z. Lai, G. Tian, X. Zhang, Z. Hou, X. Gao, W. Mi, C. Feng, M. Zeng, G. Zhou, G. Yu, G. Wu, Y. Zhou, W. Wang, X.-x. Zhang, and J. Liu, Electric-field-driven non-volatile multi-state switching of individual skyrmions in a multiferroic heterostructure, Nat. Commun. **11**, 3577 (2020).

[24] J. Liang, Q. Cui, and H. Yang, Electrically switchable Rashba-type Dzyaloshinskii-Moriya interaction and skyrmion in two-dimensional magnetoelectric multiferroics, Phys. Rev. B **102**, 220409(R) (2020).

[25] Q. Cui, J. Liang, Z. Shao, P. Cui, and H. Yang, Strain-tunable ferromagnetism and chiral spin textures in two-dimensional Janus chromium dichalcogenides, Phys. Rev. B **102**, 094425 (2020).

[26] J. Liang, W. Wang, H. Du, A. Hallal, K. Garcia, M. Chshiev, A. Fert, and H. Yang, Very large Dzyaloshinskii-Moriya interaction in two-dimensional Janus manganese dichalcogenides and its application to realize skyrmion states, Phys. Rev. B **101**, 184401 (2020).

[27] Q. Cui, J. Liang, B. Yang, Z. Wang, P. Li, P. Cui, and H. Yang, Giant enhancement of perpendicular magnetic anisotropy and induced quantum anomalous Hall effect in graphene/ $NiI_2$ heterostructures via tuning the van der Waals interlayer distance, Phys. Rev. B **101**, 214439 (2020).

[28] C. Xu, P. Chen, H. Tan, Y. Yang, H. Xiang, and L. Bellaiche, Electric-Field Switching of Magnetic Topological Charge in Type-I Multiferroics, Phys. Rev. Lett. **125**, 037203 (2020).

[29] J. Zhang, X. Shen, Y. Wang, C. Ji, Y. Zhou, J. Wang, F. Huang, and X. Lu, Design of Two-Dimensional Multiferroics with Direct Polarization-Magnetization Coupling, Phys. Rev. Lett. **125**, 017601 (2020).

[30] C.-E. Fillion, J. Fischer, R. Kumar, A. Fassatoui, S. Pizzini, L. Ranno, D. Ourdani, M. Belmeguenai, Y. Roussigné, and S.-M. Chérif, Gate-controlled skyrmion chirality, arXiv:2204.04031.

[31] X. Zhao, P. Song, C. Wang, A. C. Riis-Jensen, W. Fu, Y. Deng, D. Wan, L. Kang, S. Ning, J. Dan, T. Venkatesan, Z. Liu, W. Zhou, K. S. Thygesen, X. Luo, S. J. Pennycook, and K. P. Loh,

Engineering covalently bonded 2D layered materials by self-intercalation, Nature (London) **581**, 171 (2020).

[32] M. Huang, J. Xiang, C. Feng, H. Huang, P. Liu, Y. Wu, A. T. N'Diaye, G. Chen, J. Liang, H. Yang, J. Liang, X. Cui, J. Zhang, Y. Lu, K. Liu, D. Hou, L. Liu, and B. Xiang, Direct evidence of spin transfer torque on two-dimensional cobalt-doped $MoS_2$ ferromagnetic material, ACS Appl. Electron. Mater. **2**, 1497 (2020).

[33] W. Kohn and L. J. Sham, Self-Consistent Equations Including Exchange and Correlation Effects, Phys. Rev. **140**, A1133 (1965).

[34] G. Kresse and J. Furthmüller, Efficient iterative schemes for *ab initio* total-energy calculations using a plane-wave basis set, Phys. Rev. B **54**, 11169 (1996).

[35] G. Kresse and J. Hafner, *Ab initio* molecular dynamics for liquid metals, Phys. Rev. B **47**, 558 (1993).

[36] G. Kresse and J. Hafner, *Ab initio* molecular-dynamics simulation of the liquid-metal–amorphous-semiconductor transition in germanium, Phys. Rev. B **49**, 14251 (1994).

[37] G. Kresse and J. Furthmüller, Efficiency of ab-initio total energy calculations for metals and semiconductors using a plane-wave basis set, Comput. Mater. Sci. **6**, 15 (1996).

[38] J. P. Perdew, K. Burke, and M. Ernzerhof, Generalized Gradient Approximation Made Simple, Phys. Rev. Lett. **77**, 3865 (1996).

[39] V. I. Anisimov, F. Aryasetiawan, and A. I. Lichtenstein, First-principles calculations of the electronic structure and spectra of strongly correlated systems: The LDA $+U$ method, J. Phys.: Condens. Matter **9**, 767 (1997).

[40] L. Wang, T. Maxisch, and G. Ceder, Oxidation energies of transition metal oxides within the GGA$+U$ framework, Phys. Rev. B **73**, 195107 (2006).

[41] C. Le, S. Qin, and J. Hu, Electronic physics and possible superconductivity in layered orthorhombic cobalt oxychalcogenides, Sci. Bull. **62**, 563 (2017).

[42] S. Baroni, S. de Gironcoli, A. Dal Corso, and P. Giannozzi, Phonons and related crystal properties from density-functional perturbation theory, Rev. Mod. Phys. **73**, 515 (2001).

[43] A. Togo, F. Oba, and I. Tanaka, First-principles calculations of the ferroelastic transition between rutile-type and $CaCl_2$-type $SiO_2$ at high pressures, Phys. Rev. B **78**, 134106 (2008).

[44] A. Togo and I. Tanaka, First principles phonon calculations in materials science, Scr. Mater. **108**, 1 (2015).

[45] H. Yang, A. Thiaville, S. Rohart, A. Fert, and M. Chshiev, Anatomy of Dzyaloshinskii-Moriya Interaction at Co/Pt Interfaces, Phys. Rev. Lett. **115**, 267210 (2015).

[46] H. Yang, O. Boulle, V. Cros, A. Fert, and M. Chshiev, Controlling Dzyaloshinskii-Moriya interaction via chirality dependent atomic-layer stacking, insulator capping and electric field, Sci. Rep. **8**, 12356 (2018).

[47] O. Boulle, J. Vogel, H. Yang, S. Pizzini, D. de Souza Chaves, A. Locatelli, T. O. Menteş, A. Sala, L. D. Buda-Prejbeanu, O. Klein, M. Belmeguenai, Y. Roussigné, A. Stashkevich, S. M. Chérif, L. Aballe, M. Foerster, M. Chshiev, S. Auffret, I. M. Miron, and G. Gaudin, Room-temperature chiral magnetic skyrmions in ultrathin magnetic nanostructures, Nat. Nanotechnol. **11**, 449 (2016).

[48] H. Yang, G. Chen, A. A. C. Cotta, A. T. N'Diaye, S. A. Nikolaev, E. A. Soares, W. A. A. Macedo, K. Liu, A. K. Schmid, A. Fert, and M. Chshiev, Significant Dzyaloshinskii–Moriya interaction at graphene–ferromagnet interfaces due to the Rashba effect, Nat. Mater. **17**, 605 (2018).

[49] See Supplemental Material at http://link.aps.org/supplemental/10.1103/PhysRevB.105.174404, which includes Refs. [32,40,41,50–53], for computational details of the structures and their stabilities; ELF; calculation methods of magnetic interaction parameters $J$, $K$, and $D$; the evolution of the spin textures under an electric field; the influence of $U_{\text{eff}}$ on the magnetic parameters; magnetic parameters for micromagnetic simulations; the lattice constant; magnetic parameters; and electric polarization of other intercalated TMD bilayer multiferroelectric materials $Co(MoSe_2)_2$, $Co(MoTe_2)_2$, and $Co(WS_2)_2$.

[50] Y. Wang, J. Lv, L. Zhu, and Y. Ma, CALYPSO: A method for crystal structure prediction, Comput. Phys. Commun. **183**, 2063 (2012).

[51] D. Zhou, D. V. Semenok, D. Duan, H. Xie, W. Chen, X. Huang, X. Li, B. Liu, A. R. Oganov, and T. Cui, Superconducting praseodymium superhydrides, Sci. Adv. **6**, eaax6849 (2020).

[52] M. Yu, X. Liu, and W. Guo, Novel two-dimensional ferromagnetic semiconductors: Ga-based transition-metal trichalcogenide monolayers, Phys. Chem. Chem. Phys. **20**, 6374 (2018).

[53] P. Jiang, L. Kang, X. Zheng, Z. Zeng, and S. Sanvito, Computational prediction of a two-dimensional semiconductor $SnO_2$ with negative Poisson's ratio and tunable magnetism by doping, Phys. Rev. B **102**, 195408 (2020).

[54] T. Zhong, X. Li, M. Wu, and J.-M. Liu, Room-temperature multiferroicity and diversified magnetoelectric couplings in 2D materials, Nat. Sci. Rev. **7**, 373 (2020).

[55] G. Henkelman, B. P. Uberuaga, and H. Jónsson, A climbing image nudged elastic band method for finding saddle points and minimum energy paths, J. Chem. Phys. **113**, 9901 (2000).

[56] W. Ding, J. Zhu, Z. Wang, Y. Gao, D. Xiao, Y. Gu, Z. Zhang, and W. Zhu, Prediction of intrinsic two-dimensional ferroelectrics in $In_2Se_3$ and other III2-VI3 van der Waals materials, Nat. Commun. **8**, 14956 (2017).

[57] W. Luo, K. Xu, and H. Xiang, Two-dimensional hyperferroelectric metals: A different route to ferromagnetic-ferroelectric multiferroics, Phys. Rev. B **96**, 235415 (2017).

[58] I. Dzyaloshinsky, A thermodynamic theory of "weak" ferromagnetism of antiferromagnetics, J. Phys. Chem. Solids **4**, 241 (1958).

[59] T. Moriya, Anisotropic Superexchange Interaction and Weak Ferromagnetism, Phys. Rev. **120**, 91 (1960).

[60] A. Fert and P. M. Levy, Role of Anisotropic Exchange Interactions in Determining the Properties of Spin-Glasses, Phys. Rev. Lett. **44**, 1538 (1980).

[61] K.-W. Kim, H.-W. Lee, K.-J. Lee, and M. D. Stiles, Chirality from Interfacial Spin-Orbit Coupling Effects in Magnetic Bilayers, Phys. Rev. Lett. **111**, 216601 (2013).

[62] H. Imamura, P. Bruno, and Y. Utsumi, Twisted exchange interaction between localized spins embedded in a one- or two-dimensional electron gas with Rashba spin-orbit coupling, Phys. Rev. B **69**, 121303(R) (2004).

[63] A. Kundu and S. Zhang, Dzyaloshinskii-Moriya interaction mediated by spin-polarized band with Rashba spin-orbit coupling, Phys. Rev. B **92**, 094434 (2015).

[64] I. A. Ado, A. Qaiumzadeh, R. A. Duine, A. Brataas, and M. Titov, Asymmetric and Symmetric Exchange in a Generalized 2D Rashba Ferromagnet, Phys. Rev. Lett. **121**, 086802 (2018).

[65] H. Kronmuller, H. Kronmüller, and M. Fähnle, *Micromagnetism and the Microstructure of Ferromagnetic Solids* (Cambridge University Press, Cambridge, UK, 2003).

[66] A. Vansteenkiste and B. Van de Wiele, MuMax: A new high-performance micromagnetic simulation tool, J. Magn. Magn. Mater. **323**, 2585 (2011).

[67] B. Dupé, M. Hoffmann, C. Paillard, and S. Heinze, Tailoring magnetic skyrmions in ultra-thin transition metal films, Nat. Commun. **5**, 4030 (2014).

[68] J. Peng, Y. Liu, H. Lv, Y. Li, Y. Lin, Y. Su, J. Wu, H. Liu, Y. Guo, and Z. Zhuo, Stoichiometric two-dimensional non-van der Waals $AgCrS_2$ with superionic behaviour at room temperature, Nat. Chem. **13**, 1235 (2021).